

Predictions for the Sivers Single-Spin Asymmetry from Holographic QCD

Valery E. Lyubovitskij,^{1,2,3} Ivan Schmidt,² and Stanley J. Brodsky⁴

¹*Institut für Theoretische Physik, Universität Tübingen,*

Kepler Center for Astro and Particle Physics, Auf der Morgenstelle 14, D-72076 Tübingen, Germany

²*Departamento de Física y Centro Científico Tecnológico de Valparaíso-CCTVal,*

Universidad Técnica Federico Santa María, Casilla 110-V, Valparaíso, Chile

³*Millennium Institute for Subatomic Physics at the High-Energy Frontier (SAPHIR) of ANID,*

Fernández Concha 700, Santiago, Chile

⁴*SLAC National Accelerator Laboratory, Stanford University, Stanford, CA 94309, USA*

A new approach to nonperturbative QCD, *holographic light-front QCD*, provides a comprehensive model for hadron dynamics and spectroscopy, incorporating color confinement, a universal hadron mass scale, the prediction of a massless pion in the chiral limit, and connections between the spectroscopy of mesons, baryons and tetraquarks across the full hadron spectrum. In this article we present predictions for the Sivers asymmetry and related transverse momentum distributions for the proton based on the light-front wavefunctions of the baryon eigenstate predicted by holographic QCD.

A novel approach to nonperturbative QCD dynamics, *holographic light-front QCD* [1, 2], has led to effective semiclassical relativistic bound-state equations for hadrons of arbitrary spin; it incorporates fundamental hadronic properties which are not apparent from the QCD Lagrangian, including color confinement, the emergence of a universal hadron mass scale, the prediction of a massless pion in the chiral limit, and remarkable connections between the spectroscopy of mesons, baryons and tetraquarks across the full hadronic spectrum. The light-front (LF) holographic formalism is based on the combination of superconformal quantum mechanics [3, 4], light-front quantization [5], and the holographic embedding on a higher dimensional gravity theory [6] (gauge/gravity correspondence), leading to new analytic insights into the structure of hadrons and their dynamics.

Holographic QCD also provides analytic predictions for the boost invariant light-front wave functions (LFWFs) $\psi_H(x_i, k_{\perp i}, \lambda_i)$ of each hadronic eigenstate, the solutions of the light-front Schrödinger equations. The knowledge of the LFWFs allows one to predict dynamical properties of the hadrons such as form factors, the distribution amplitudes underlying exclusive hadronic amplitudes, the structure functions underlying deep inelastic processes, etc. [1, 2, 7–12].

In this paper we will use the LF Holographic QCD approach to predict the Sivers asymmetry as formulated in Ref. [13]. In particular, it was shown [13] that a single-spin asymmetry (SSA) in the semi-inclusive deep inelastic (SIDIS) electroproduction $\gamma^*p \rightarrow HX$ arises from final-state interactions. We will focus on the subprocess of the lepton SIDIS process $\ell p^\uparrow \rightarrow \ell' HX$ shown in Fig. 1, where the quark jet produces a leading pion, including the final-state interactions arising from gluonic exchange. In LF Holography, the valence state of the proton is the bound state of struck u quark and a scalar spectator diquark $[ud]_0$ — the quark-diquark model of nucleon. The interference of tree and one-loop graphs (see Fig. 2) contributing to the electroproduction reaction $\gamma^*p \rightarrow u[ud]_0$ generates the single-spin asymmetry (SSA) of the proton [13].

The first experimental measurement of the Sivers effect was performed by the HERMES Collaboration at DESY in the study of the electroproduction of pion in the SIDIS on the transversally polarized hydrogen gas target [14] and was later confirmed in Ref. [15]. Then, in Refs. [16, 17] the COMPASS Collaboration at SPS CERN reported results on the Collins and Sivers asymmetries for charged hadrons produced in SIDIS of high energy muons on transversely polarized proton and deuteron targets. Later, in Ref. [18] the Jefferson Lab Hall A Collaboration presented the first measurement of SSA in the SIDIS reaction $^3H(e, e', \pi^\pm, X)$ using transversely polarized target. For recent results of the COMPASS Collaboration, where Sivers asymmetries were extracted in SIDIS at the hard scales, see Refs. [19, 20]. Since prediction of the Sivers asymmetry in Ref. [13] big theoretical progress was achieved in further detailed understanding of this phenomena (see, e.g., Refs. [21]–[38]). A main advantage of the study of the Sivers asymmetry is its detailed access to the transverse momentum distribution function (TMD) and its spin-weighted moments. As has been stressed in Ref. [36], the model for the LFWFs was taken from Ref. [10]. After Ref. [10] we sufficiently improved the parametrization of the LFWFs to guarantee that the calculated parton distributions of the hadrons are consistent with model-independent scaling at large x . In particular, in Ref. [9], which studies nucleon parton distributions and form factors, we showed that the parametrization of the LFWFs in terms of combinations of unpolarized and polarized PDFs produce the correct scaling for both the PDFs (by construction) as well as the TMDs and GPDs. The resulting nucleon form factors also obey the model-independent power scalings at large Q^2 discovered by Brodsky-Farrar-Matveev-Muradyan-Tavkhelidze [39]. Later in series of papers (see Refs. [7, 8, 11, 12]), a more accurate setup for the LFWFs, consistent with model-independent constraints in QCD, were successfully applied including gluon parton densities. Note that the model for nucleon LFWFs proposed in Ref. [10] and used in Ref. [36] is not fully consistent with QCD constraints. That is why we have carried out the further improvements.

We would also like to stress that the framework in Ref. [36] for the calculation of the asymmetries in SIDIS is also not fully consistent. In particular, the authors of Ref. [36] do not calculate the fragmentation functions and use a phenomenological input, while these functions can be calculated directly in LF QCD as the other types of parton distribution. It is our main purpose that starting from the present paper, we intend to do a comprehensive analysis of the asymmetries in QCD processes at fixed targets, like Drell-Yan and SIDIS.

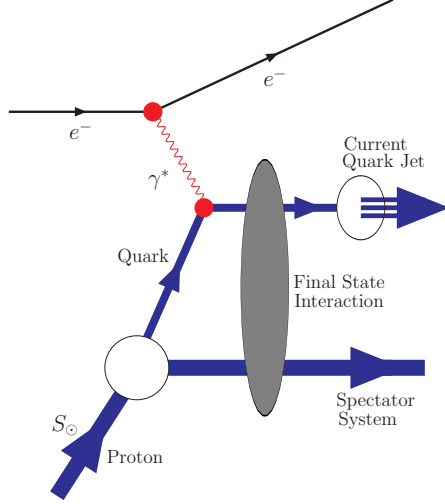


FIG. 1: Final-state interaction in the lepton SIDIS process $\ell p^\uparrow \rightarrow \ell' H X$.

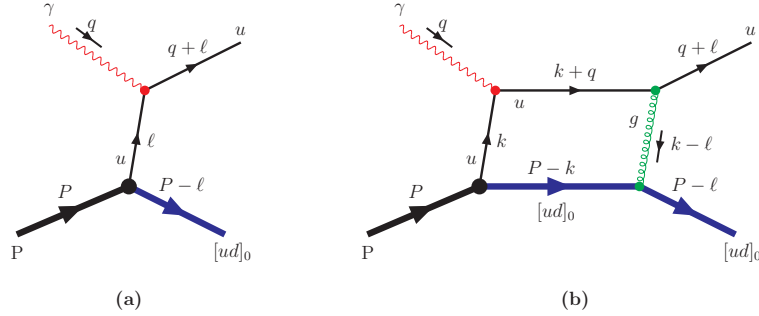


FIG. 2: Tree (a) and one-loop (b) diagrams contributing to the electroproduction process $\gamma^* p \rightarrow u[ud]_0$.

We start with basic notions of Holographic QCD approach based on quark-scalar diquark structure of nucleon. The $J^z = +\frac{1}{2}$ two-particle quark-scalar diquark Fock state is given by [9, 10, 12, 13, 40, 41]:

$$\left| \Psi^\uparrow(P^+, \mathbf{0}_\perp) \right\rangle = \int \frac{d^2 \mathbf{k}_\perp dx}{16\pi^3 \sqrt{x(1-x)}} \left[\varphi_{+\frac{1}{2}}^\uparrow(x, \mathbf{k}_\perp) \left| +\frac{1}{2}; xP^+, \mathbf{k}_\perp \right\rangle + \varphi_{-\frac{1}{2}}^\uparrow(x, \mathbf{k}_\perp) \left| -\frac{1}{2}; xP^+, \mathbf{k}_\perp \right\rangle \right] \quad (1)$$

where we use notation $\varphi_{\lambda_u}^{\lambda_N}(x, \mathbf{k}_\perp)$ for the light-front wave function (LFWF) at the initial scale μ_0 with specific helicities for the proton $\lambda_N = \uparrow$ and \downarrow and for the struck quark $\lambda_u = +\frac{1}{2}$ and $-\frac{1}{2}$ [9, 10, 12]:

$$\begin{aligned} \varphi_{+\frac{1}{2}}^\uparrow(x, \mathbf{k}_\perp) &= \frac{2\pi\sqrt{2}}{\kappa} \sqrt{u_{v+}(x)} \exp\left[-\frac{\mathbf{k}_\perp^2}{2\kappa^2}\right], \\ \varphi_{-\frac{1}{2}}^\uparrow(x, \mathbf{k}_\perp) &= -\frac{2\pi\sqrt{2}}{\kappa^2} (k^1 + ik^2) \sqrt{u_{v-}(x)} \exp\left[-\frac{\mathbf{k}_\perp^2}{2\kappa^2}\right], \end{aligned} \quad (2)$$

where $u_{v\pm}(x) = u_v(x) \pm \delta u_v(x)$, $u_v(x)$ and $\delta u_v(x)$ are the helicity-independent (unpolarized) and helicity-dependent (polarized) u valence quark parton distributions, $\kappa \sim 350 - 500$ MeV is the scale dilaton parameter.

In a similar way one can construct the $J^z = -1/2$ quark-scalar diquark Fock state components:

$$\begin{aligned}\varphi_{+\frac{1}{2}}^\downarrow(x, \mathbf{k}_\perp) &= \frac{2\pi\sqrt{2}}{\kappa^2} (k^1 - ik^2) \sqrt{u_{v-}(x)} \exp\left[-\frac{\mathbf{k}_\perp^2}{2\kappa^2}\right], \\ \varphi_{-\frac{1}{2}}^\downarrow(x, \mathbf{k}_\perp) &= \frac{2\pi\sqrt{2}}{\kappa} \sqrt{u_{v+}(x)} \exp\left[-\frac{\mathbf{k}_\perp^2}{2\kappa^2}\right].\end{aligned}\quad (3)$$

The wave functions $\varphi_{\pm\frac{1}{2}}^\uparrow(x, \mathbf{k}_\perp)$ and $\varphi_{\pm\frac{1}{2}}^\downarrow(x, \mathbf{k}_\perp)$ are normalized in a such way that their combinations produce helicity-independent and helicity-dependent u -quark PDFs in the proton:

$$\begin{aligned}u_v(x) &= \int \frac{d^2\mathbf{k}_\perp}{16\pi^3} \left[|\varphi_{+\frac{1}{2}}^\uparrow(x, \mathbf{k}_\perp)|^2 + |\varphi_{-\frac{1}{2}}^\uparrow(x, \mathbf{k}_\perp)|^2 \right] \\ &= \int \frac{d^2\mathbf{k}_\perp}{16\pi^3} \left[|\varphi_{+\frac{1}{2}}^\downarrow(x, \mathbf{k}_\perp)|^2 + |\varphi_{-\frac{1}{2}}^\downarrow(x, \mathbf{k}_\perp)|^2 \right],\end{aligned}\quad (4)$$

$$\begin{aligned}\delta u_v(x) &= \int \frac{d^2\mathbf{k}_\perp}{16\pi^3} \left[|\varphi_{+\frac{1}{2}}^\uparrow(x, \mathbf{k}_\perp)|^2 - |\varphi_{-\frac{1}{2}}^\uparrow(x, \mathbf{k}_\perp)|^2 \right] \\ &= \int \frac{d^2\mathbf{k}_\perp}{16\pi^3} \left[|\varphi_{-\frac{1}{2}}^\downarrow(x, \mathbf{k}_\perp)|^2 - |\varphi_{+\frac{1}{2}}^\downarrow(x, \mathbf{k}_\perp)|^2 \right].\end{aligned}\quad (5)$$

Note that in the original version of the quark-scalar diquark model [13, 40, 41] by construction the proton LFWFs $|u[ud]_0\rangle$ has $L = 0$ and $L = 1$ components with equal probability. In Ref. [9] it was proposed to relate them with two combinations of valence quark PDFs. It led to not equal probabilities of the $L = 0$ and $L = 1$ components.

Next we define four possible spin-spin transitions between proton and struck quark:

$$\begin{aligned}\uparrow\left(J_p^z = +\frac{1}{2}\right) &\rightarrow \uparrow\left(J_q^z = +\frac{1}{2}\right), \\ \downarrow\left(J_p^z = -\frac{1}{2}\right) &\rightarrow \uparrow\left(J_q^z = +\frac{1}{2}\right), \\ \uparrow\left(J_p^z = +\frac{1}{2}\right) &\rightarrow \downarrow\left(J_q^z = -\frac{1}{2}\right), \\ \downarrow\left(J_p^z = -\frac{1}{2}\right) &\rightarrow \downarrow\left(J_q^z = -\frac{1}{2}\right).\end{aligned}\quad (6)$$

The corresponding amplitudes \mathcal{A} including both tree and one-loop contributions have been calculated in Ref. [13] using diquark model. Here, we present our results for the \mathcal{A} 's using Holographic QCD:

$$\begin{aligned}\mathcal{A}(\uparrow\rightarrow\uparrow) &= C^+(\Delta) h(\ell_\perp^2) e^{i\chi_1}, \\ \mathcal{A}(\downarrow\rightarrow\uparrow) &= \frac{\ell^1 - i\ell^2}{\kappa} C^-(\Delta) h(\ell_\perp^2) e^{i\chi_2}, \\ \mathcal{A}(\uparrow\rightarrow\downarrow) &= -\frac{\ell^1 + i\ell^2}{\kappa} C^-(\Delta) h(\ell_\perp^2) e^{i\chi_2}, \\ \mathcal{A}(\downarrow\rightarrow\downarrow) &= C^+(\Delta) h(\ell_\perp^2) e^{i\chi_1}.\end{aligned}\quad (7)$$

Here

$$\begin{aligned}C^\pm(\Delta) &= 2P^+ g e_u \left(u_{v\pm}(\Delta) \Delta(1-\Delta) \right)^{1/2}, \\ h(\ell_\perp^2) &= \frac{2\pi\sqrt{2}}{\kappa} \exp\left[-\frac{\ell_\perp^2}{2\kappa^2}\right].\end{aligned}\quad (8)$$

and $\chi_{1,2}$ are the rescattering phases taking into account one-loop contributions [13]:

$$\chi_i = \frac{\alpha_s C_F}{2} g_i, \quad (9)$$

g is the coupling of proton and $u[ud]_0$ quark-scalar diquark state, $\Delta = k^+/P^+$, $\ell_\perp = (\ell^x, \ell^y)$, and $\alpha_s = \alpha_s(\mu^2) = 4\pi\beta_0/\log(\mu^2/\Lambda_{\text{QCD}}^2)$ is the QCD coupling at the scale μ , $C_F = 4/3$, $\beta_0 = 9$, $\Lambda_{\text{QCD}} = 0.226$ GeV. As shown in Eq. (3)

we have parametrized the LFWFs in terms of combinations of quark PDFs $u_{v\pm}$, instead of the simple ansatz of the original spectator model. Therefore, in Eq. (3) the combination u_{v+} appears in the case of the spin-spin transitions without flip, while u_{v-} appears in case of the spin-spin transitions with spin flip. Therefore, the C^+ is proportional to u_{v+} and C^- to u_{v-} .

The loop couplings g_1 and g_2 have been calculated in in Ref. [13]. It was shown that, while g_1 and g_2 depend in the infrared regulator λ_g (gluon mass), their difference is independent of λ_g and, therefore, is infrared finite:

$$\begin{aligned}\Delta g &= g_1 - g_2 = \frac{\kappa^2}{\ell_\perp^2} \log \frac{\ell_\perp^2 + B(\Delta)}{B(\Delta)}, \\ B(\Delta) &= m^2(1 - \Delta) + m_{[ud]}^2 \Delta - M_N^2 \Delta(1 - \Delta),\end{aligned}\quad (10)$$

where m and $m_{[ud]}$ are the constituent masses of struck u quark and spectator diquark $[ud]_0$, M_N is the nucleon mass.

Note, the Δ contributes to the azimuthal single-spin asymmetry transverse to the production plane [13]:

$$\mathcal{P}_y = \alpha_s C_F \frac{\ell^x}{\kappa} \frac{\Delta g \sqrt{1 - R^2(\Delta)}}{1 + R(\Delta) + \frac{\ell_\perp^2}{\kappa^2}(1 - R(\Delta))}, \quad (11)$$

where $R(\Delta) = \delta u_v(\Delta)/u_v(\Delta)$. The novel result is that we expressed the \mathcal{P}_y asymmetry through the ratio of the valence PDFs of the u quark — δu_v and u_v .

Next, following Ref. [32] we can calculate the Sivers $f_{1T}^\perp(x, \mathbf{k}_\perp)$ and Boer-Mulders $h_1^\perp(x, \mathbf{k}_\perp)$ T-odd u -quark TMDs. First, we update the LFWFs including rescattering phases $\chi_{1,2}$ due to final state interactions [32]:

$$\begin{aligned}\Phi_{+\frac{1}{2}}^\uparrow(x, \mathbf{k}_\perp) &= \varphi_{+\frac{1}{2}}^\uparrow(x, \mathbf{k}_\perp) e^{i\chi_1}, \\ \Phi_{-\frac{1}{2}}^\uparrow(x, \mathbf{k}_\perp) &= \varphi_{-\frac{1}{2}}^\uparrow(x, \mathbf{k}_\perp) e^{i\chi_2}, \\ \Phi_{+\frac{1}{2}}^\downarrow(x, \mathbf{k}_\perp) &= \varphi_{+\frac{1}{2}}^\downarrow(x, \mathbf{k}_\perp) e^{i\chi_2}, \\ \Phi_{-\frac{1}{2}}^\downarrow(x, \mathbf{k}_\perp) &= \varphi_{-\frac{1}{2}}^\downarrow(x, \mathbf{k}_\perp) e^{i\chi_1}.\end{aligned}\quad (12)$$

Second, we use the light-front decomposition for the Sivers and Boer-Mulders functions in terms of the LFWFs from Eq. (12):

$$\begin{aligned}\frac{k^x}{M_N} f_{1T}^{\perp u}(x, \mathbf{k}_\perp) &\equiv -\frac{i}{32\pi^3} \left[\Phi_{+\frac{1}{2}}^{\uparrow\uparrow}(x, \mathbf{k}_\perp) \Phi_{+\frac{1}{2}}^\downarrow(x, \mathbf{k}_\perp) + \Phi_{-\frac{1}{2}}^{\uparrow\uparrow}(x, \mathbf{k}_\perp) \Phi_{-\frac{1}{2}}^\downarrow(x, \mathbf{k}_\perp) \right. \\ &\quad \left. - \Phi_{-\frac{1}{2}}^{\uparrow\downarrow}(x, \mathbf{k}_\perp) \Phi_{-\frac{1}{2}}^\uparrow(x, \mathbf{k}_\perp) - \Phi_{+\frac{1}{2}}^{\uparrow\downarrow}(x, \mathbf{k}_\perp) \Phi_{+\frac{1}{2}}^\uparrow(x, \mathbf{k}_\perp) \right],\end{aligned}\quad (13)$$

$$\begin{aligned}\frac{k^x}{M_N} h_1^{\perp u}(x, \mathbf{k}_\perp) &= -\frac{i}{32\pi^3} \left[\Phi_{-\frac{1}{2}}^{\uparrow\uparrow}(x, \mathbf{k}_\perp) \Phi_{+\frac{1}{2}}^\uparrow(x, \mathbf{k}_\perp) - \Phi_{+\frac{1}{2}}^{\uparrow\uparrow}(x, \mathbf{k}_\perp) \Phi_{-\frac{1}{2}}^\uparrow(x, \mathbf{k}_\perp) \right. \\ &\quad \left. + \Phi_{-\frac{1}{2}}^{\uparrow\downarrow}(x, \mathbf{k}_\perp) \Phi_{+\frac{1}{2}}^\downarrow(x, \mathbf{k}_\perp) - \Phi_{+\frac{1}{2}}^{\uparrow\downarrow}(x, \mathbf{k}_\perp) \Phi_{-\frac{1}{2}}^\downarrow(x, \mathbf{k}_\perp) \right].\end{aligned}\quad (14)$$

We get

$$f_{1T}^{\perp u}(x, \mathbf{k}_\perp) \equiv h_1^{\perp u}(x, \mathbf{k}_\perp) = -\frac{\alpha_s C_F}{2\pi\kappa^3} M_N \Delta g \sqrt{u_v^2(x) - \delta u_v^2(x)} \exp\left[-\frac{\mathbf{k}_\perp^2}{\kappa^2}\right]. \quad (15)$$

Using our result for the unpolarized TMD $f_1(x, \mathbf{k}_\perp)$ [9]:

$$\begin{aligned}f_1^u(x, \mathbf{k}_\perp) &= \frac{1}{32\pi^3} \left[|\Phi_{+\frac{1}{2}}^\uparrow(x, \mathbf{k}_\perp)|^2 + |\Phi_{+\frac{1}{2}}^\downarrow(x, \mathbf{k}_\perp)|^2 + |\Phi_{-\frac{1}{2}}^\uparrow(x, \mathbf{k}_\perp)|^2 + |\Phi_{-\frac{1}{2}}^\downarrow(x, \mathbf{k}_\perp)|^2 \right] \\ &= \frac{1}{2\pi\kappa^2} \left[u_v(x) + \delta u_v(x) + \frac{\mathbf{k}_\perp^2}{\kappa^2} (u_v(x) - \delta u_v(x)) \right] \exp\left[-\frac{\mathbf{k}_\perp^2}{\kappa^2}\right]\end{aligned}\quad (16)$$

we reproduce the well-known relation between the asymmetry \mathcal{P}_y and TMDs $f_1^u(x, \mathbf{k}_\perp)$ and $f_{1T}^{\perp u}(x, \mathbf{k}_\perp)$ [22, 24]:

$$\mathcal{P}_y = -\frac{\ell^x}{M_N} \frac{f_{1T}^{\perp u}(\Delta, \ell_\perp)}{f_1^u(\Delta, \ell_\perp)}. \quad (17)$$

Notice that the results for the d -quark TMDs are obtained upon replacement $u_v(x) \rightarrow d_v(x)$ and $\delta u_v(x) \rightarrow \delta d_v(x)$ and changing overall sign in $\varphi_{-\frac{1}{2}}^\uparrow(x, \mathbf{k}_\perp)$ and $\varphi_{+\frac{1}{2}}^\downarrow(x, \mathbf{k}_\perp)$ [9]. One gets:

$$f_1^d(x, \mathbf{k}_\perp) = \frac{1}{2\pi\kappa^2} \left[d_v(x) + \delta d_v(x) + \frac{\mathbf{k}_\perp^2}{\kappa^2} (d_v(x) - \delta d_v(x)) \right] \exp \left[-\frac{\mathbf{k}_\perp^2}{\kappa^2} \right],$$

$$f_{1T}^{\perp d}(x, \mathbf{k}_\perp) \equiv h_1^{\perp d}(x, \mathbf{k}_\perp) = \frac{\alpha_s C_F}{2\pi\kappa^3} M_N \Delta g \sqrt{d_v^2(x) - \delta d_v^2(x)} \exp \left[-\frac{\mathbf{k}_\perp^2}{\kappa^2} \right]. \quad (18)$$

Note, that in the scalar quark-diquark model, the relations between the Siverson and Boer-Mulders functions for both flavors (u and d quarks) have the same sign [30, 32]. It is true that inclusion of the axial-vector diquark will distinguish the relations for u and d quark. See Refs. [30, 32].

Now we present our numerical results for the Siverson asymmetry and TMDs. In our analysis, we will use the following set of parameters: $\mu_0^2 = 0.40 \text{ GeV}^2$ is the initial scale, $M_N = 0.93827 \text{ GeV}$ is the nucleon mass, $m = 0.35 \text{ GeV}$ is the constituent mass of u and d quark, and $\kappa = 0.5 \text{ GeV}$ is the dilaton scale parameter. The mass of the $[ud]_0$ scalar diquark $m_{[ud]}$ will be varied from 0.65 to 0.8 GeV. For the q_v and δq_v ($q = u, d$) quark PDFs and the ratio $R(x) = \delta u_v(x)/u_v(x)$ we use the results of the Glück-Reya-Vogt (GRV)/Glück-Reya-Stratmann-Vogelsang (GRSV) fit done in Refs. [42, 43]. In particular, $R(x) \simeq 2.043 x^{0.97} (1-x)^{0.64}$.

TABLE I: First moments of the Siverson TMDs for u and d quark

x	$Q^2 \text{ (GeV}^2\text{)}$	$ x f_{1T}^{\perp(1)u}(x) $		$ x f_{1T}^{\perp(1)d}(x) $	
		COMPASS [20]	Our results	COMPASS [20]	Our results
0.0063	1.27	$ 0.0022 \pm 0.0051 $	0.0004 ± 0.0001	$ 0.001 \pm 0.021 $	0.0002 ± 0.00001
0.0105	1.55	$ 0.0029 \pm 0.0040 $	0.0007 ± 0.0001	$ 0.004 \pm 0.017 $	0.0003 ± 0.0001
0.0164	1.83	0.0058 ± 0.0037	0.0013 ± 0.0002	0.019 ± 0.015	0.0005 ± 0.0001
0.0257	2.17	0.0097 ± 0.0033	0.0022 ± 0.0003	0.034 ± 0.013	0.0008 ± 0.0002
0.0399	2.82	0.0179 ± 0.0036	0.004 ± 0.005	0.032 ± 0.015	0.0014 ± 0.0003
0.0629	4.34	0.0224 ± 0.0046	0.007 ± 0.001	0.048 ± 0.019	0.0025 ± 0.0005
0.101	6.76	0.0171 ± 0.0057	0.012 ± 0.003	0.025 ± 0.023	0.004 ± 0.001
0.163	10.6	0.0295 ± 0.0070	0.018 ± 0.004	0.056 ± 0.027	0.006 ± 0.002
0.288	20.7	0.0160 ± 0.0073	0.019 ± 0.006	$ 0.017 \pm 0.028 $	0.005 ± 0.002

In Fig. 3 we show two-dimensional plots for the \mathcal{P}_y asymmetry as function of Δ variable at $|\ell_\perp| = 0.5 \text{ GeV}$ $|\ell_\perp| = 0.15 \text{ GeV}$. The shaded bands correspond to a variation of the $m_{[ud]} = 0.65 - 0.8 \text{ GeV}$. Increasing of $m_{[ud]}$ leads to a suppression of the asymmetry \mathcal{P}_y . In Fig. 4 we present three-dimensional plots for the \mathcal{P}_y as function of two variables Δ and $|\ell_\perp|$ running from 0 to 1 and to 0.15 to 0.5 GeV, respectively, at two typical (low and upper) values of the scalar diquark mass $m_{[ud]} = 0.65$ and 0.8 GeV .

In Figs. 5-10 we present our results for the u and d quark Siverson TMDs and for their first and 1/2 moments:

$$f_{1T}^{\perp(1)q}(x) = \int d^2\mathbf{k}_\perp \frac{\mathbf{k}_\perp^2}{2M_N^2} f_{1T}^{\perp q}(x, \mathbf{k}_\perp)$$

$$= -\alpha_s C_F \frac{\kappa}{4M_N} n_q \sqrt{q_v^2(x) - \delta q_v^2(x)} \Gamma[0, b(x)] \exp[b(x)],$$

$$f_{1T}^{\perp(1/2)q}(x) = \int d^2\mathbf{k}_\perp \frac{|\mathbf{k}_\perp|}{M_N} f_{1T}^{\perp q}(x, \mathbf{k}_\perp)$$

$$= -\alpha_s C_F n_q \sqrt{q_v^2(x) - \delta q_v^2(x)} \int_0^\infty dt \exp[-t^2] \log \frac{t^2 + b(x)}{b(x)}, \quad (19)$$

where $n_u = 1$, $n_d = -1$, $b(x) = B(x)/\kappa^2$,

$$\Gamma[a, z] = \int_z^\infty dt t^{a-1} e^{-t} \quad (20)$$

is the incomplete Gamma function. In particular, in Figs. 5 and 6 we show our predictions for the Siverts TMD $xf_{1T}^{\perp u}(x, \mathbf{k}_{\perp})$ and $xf_{1T}^{\perp d}(x, \mathbf{k}_{\perp})$ as functions of x at $|\mathbf{k}_{\perp}| = 0.5$ and 0.15 GeV. In Figs. 7 and 8 we display three-dimensional plots for the Siverts TMDs $|f_{1T}^{\perp u}(x, \mathbf{k}_{\perp})|$ and $|f_{1T}^{\perp d}(x, \mathbf{k}_{\perp})|$ as a functions of x and \mathbf{k}_{\perp}^2 for $m_{[ud]} = 0.65$ and 0.8 GeV. Finally, in Figs. 9 and 10 we present our results for the first and $1/2$ moments of the Siverts TMDs.

In Table I we compare our results for the magnitudes of the first moments of the Siverts TMDs for u and d quarks $|xf_{1T}^{\perp(1)u,d}(x)|$ with data extracted by the COMPASS Collaboration [20] at different scales of resolution Q^2 . Note, that our results for the moments of the Siverts quark TMDs are in good agreement with results of other theoretical approaches (see, e.g, compilation of theoretical predictions in Ref. [26]).

In conclusion, we have presented predictions for the Siverts asymmetry and TMDs based on holographic QCD. These results will provide an important test of this novel approach to nonperturbative hadron dynamics.

Acknowledgments

This work was funded by BMBF (Germany) “Verbundprojekt 05P2021 (ErUM-FSP T01) - Run 3 von ALICE am LHC: Perturbative Berechnungen von Wirkungsquerschnitten für ALICE” (Förderkennzeichen: 05P21VTCAA), by ANID PIA/APOYO AFB180002 (Chile), by FONDECYT (Chile) under Grant No. 1191103 and by ANID–Millennium Program–ICN2019_044 (Chile). The work of S.J.B. was supported in part by the Department of Energy under contract DE-AC02-76SF00515. SLAC-PUB-17676.

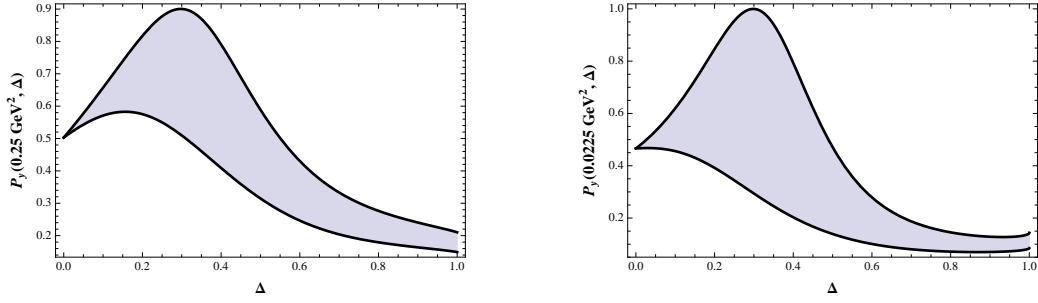


FIG. 3: 2D plots of the \mathcal{P}_y asymmetry as function of Δ at $|\ell_\perp| = 0.5$ GeV (left panel) and $|\ell_\perp| = 0.15$ GeV (right panel).

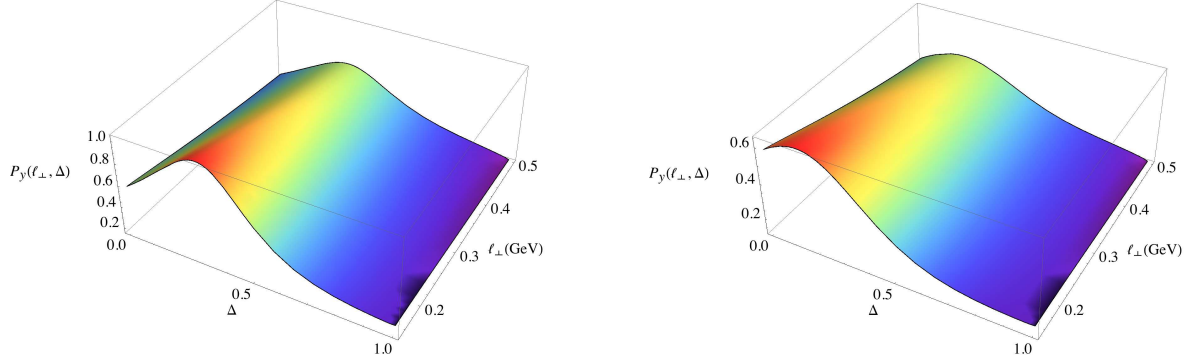


FIG. 4: 3D plots of the \mathcal{P}_y asymmetry as function of Δ and $|\ell_\perp|$ for $m_{[ud]} = 0.65$ GeV (left panel) and for $m_{[ud]} = 0.8$ GeV (right panel).

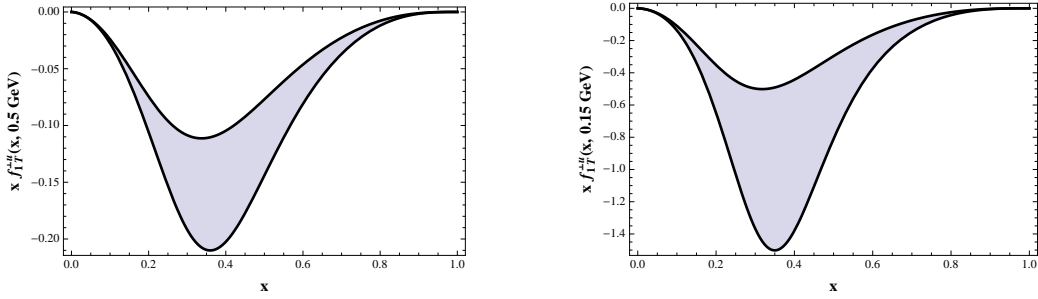


FIG. 5: 2D plots of the Siverts TMD $x f_{1T}^{\perp u}(x, \mathbf{k}_\perp)$ as function of x at $|\mathbf{k}_\perp| = 0.5$ GeV (left panel) and $|\mathbf{k}_\perp| = 0.15$ GeV (right panel).

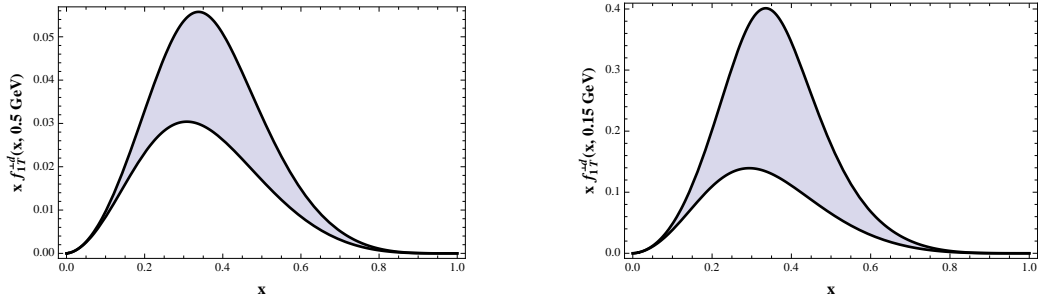


FIG. 6: 2D plots of the Siverts TMD $x f_{1T}^{\perp d}(x, \mathbf{k}_\perp)$ as function of x at $|\mathbf{k}_\perp| = 0.5$ GeV (left panel) and $|\mathbf{k}_\perp| = 0.15$ GeV (right panel).

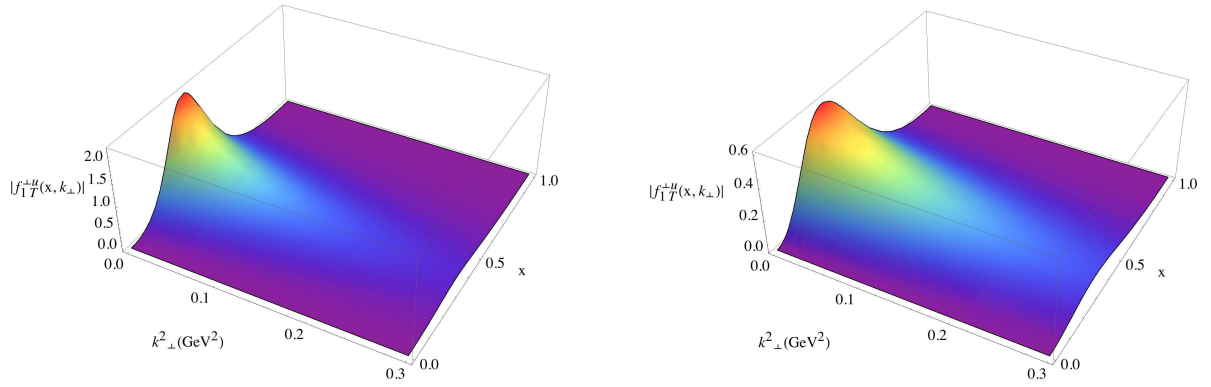


FIG. 7: 3D plots of the Siverts TMD $|xf_{1T}^{\perp u}(x, \mathbf{k}_{\perp})|$ as function of x and k_{\perp}^2 for $m_{[ud]} = 0.65$ GeV (left panel) and for $m_{[ud]} = 0.8$ GeV (right panel).

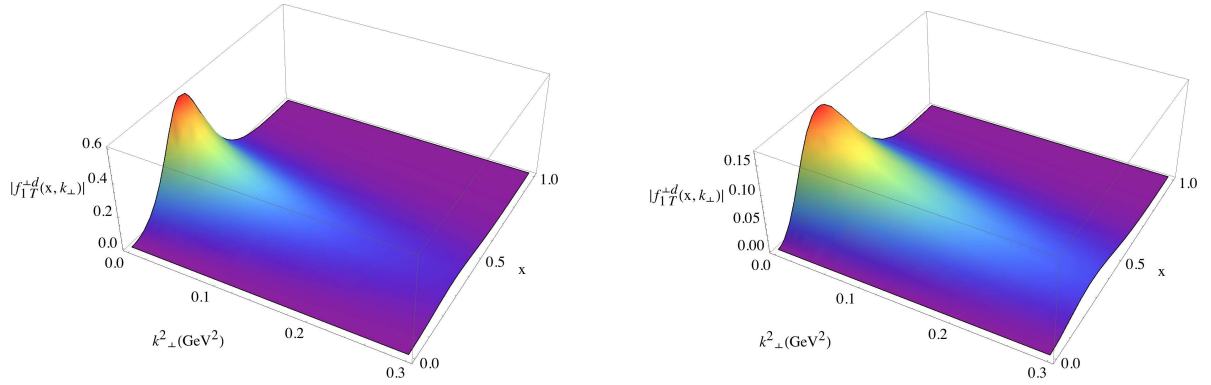


FIG. 8: 3D plots of the Siverts TMD $|xf_{1T}^{\perp d}(x, \mathbf{k}_{\perp})|$ as function of x and k_{\perp}^2 for $m_{[ud]} = 0.65$ GeV (left panel) and for $m_{[ud]} = 0.8$ GeV (right panel).

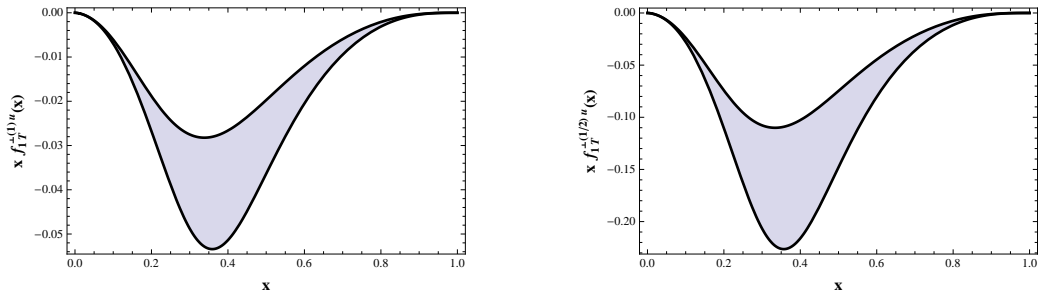


FIG. 9: 2D plots of the moments of the Siverts TMD $xf_{1T}^{\perp(1)u}(x)$ and $xf_{1T}^{\perp(1/2)u}(x)$.

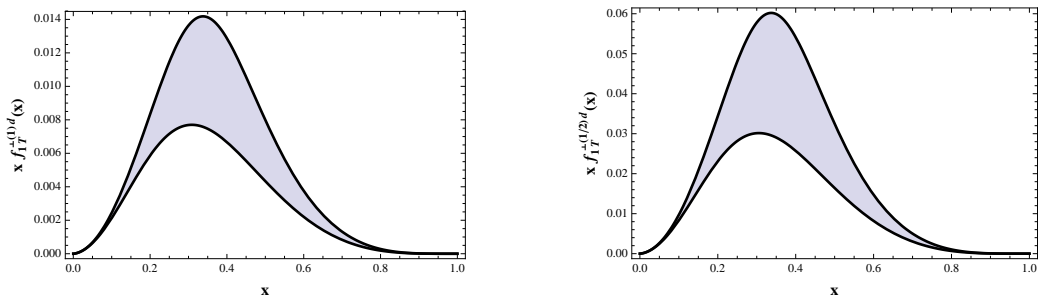


FIG. 10: 2D plots of the moments of the Siverts TMD $xf_{1T}^{\perp(1)d}(x)$ and $xf_{1T}^{\perp(1/2)d}(x)$.

-
- [1] S. J. Brodsky, G. F. de Teramond, H. G. Dosch, and J. Erlich, Phys. Rept. **584**, 105 (2015).
- [2] S. J. Brodsky and G. F. de Teramond, Phys. Rev. D **77**, 056007 (2008).
- [3] V. de Alfaro, S. Fubini, and G. Furlan, Nuovo Cim. A **34**, 569 (1976).
- [4] S. Fubini and E. Rabinovici, Nucl. Phys. B **245**, 17 (1984).
- [5] P. A. M. Dirac, Rev. Mod. Phys. **21**, 392 (1949).
- [6] J. M. Maldacena, Adv. Theor. Math. Phys. **2**, 231 (1998).
- [7] R. S. Sufian, G. F. de Téramond, S. J. Brodsky, A. Deur, and H. G. Dosch, Phys. Rev. D **95**, 014011 (2017).
- [8] G. F. de Téramond, T. Liu, R. S. Sufian, H. G. Dosch, S. J. Brodsky, and A. Deur (HLFHS Collaboration), Phys. Rev. Lett. **120**, 182001 (2018).
- [9] T. Gutsche, V. E. Lyubovitskij, and I. Schmidt, Eur. Phys. J. C **77**, 86 (2017).
- [10] T. Gutsche, V. E. Lyubovitskij, I. Schmidt, and A. Vega, Phys. Rev. D **89**, 054033 (2014); D **92**, 019902(E) (2015); D **91**, 054028 (2015).
- [11] V. E. Lyubovitskij and I. Schmidt, Phys. Rev. D **103**, 094017 (2021); D **104**, 014001 (2021).
- [12] V. E. Lyubovitskij and I. Schmidt, Phys. Rev. D **102**, 034011 (2020).
- [13] S. J. Brodsky, D. S. Hwang, and I. Schmidt, Phys. Lett. B **530**, 99 (2002).
- [14] A. Airapetian *et al.* (HERMES Collaboration), Phys. Rev. Lett. **94**, 012002 (2005).
- [15] A. Airapetian *et al.* (HERMES Collaboration), Phys. Rev. Lett. **103**, 152002 (2009).
- [16] V. Y. Alexakhin *et al.* (COMPASS Collaboration), Phys. Rev. Lett. **94**, 202002 (2005); E. S. Ageev *et al.* (COMPASS Collaboration), Nucl. Phys. B **765**, 31 (2007).
- [17] M. G. Alekseev *et al.* (COMPASS Collaboration), Phys. Lett. B **692**, 240 (2010); C. Adolph *et al.* (COMPASS Collaboration), Phys. Lett. B **717**, 383 (2012).
- [18] X. Qian *et al.* (Jefferson Lab Hall A Collaboration), Phys. Rev. Lett. **107**, 072003 (2011).
- [19] C. Adolph *et al.* (COMPASS Collaboration), Phys. Lett. B **770**, 138 (2017).
- [20] M. G. Alexeev *et al.* (COMPASS Collaboration), Nucl. Phys. B **940**, 34 (2019).
- [21] S. J. Brodsky, D. S. Hwang, and I. Schmidt, Phys. Lett. B **553**, 223 (2003);
- [22] S. J. Brodsky, D. S. Hwang, and I. Schmidt, Nucl. Phys. B **642**, 344 (2002).
- [23] J. C. Collins, Phys. Lett. B **536**, 43 (2002).
- [24] B. Boer, S. J. Brodsky, and D. S. Hwang, Phys. Rev. D **67**, 054003 (2003).
- [25] A. V. Efremov, K. Goeke, and P. Schweitzer, Phys. Lett. B **568**, 63 (2003); A. V. Efremov, K. Goeke, S. Menzel, A. Metz, and P. Schweitzer, Phys. Lett. B **612**, 233 (2005); J. C. Collins, A. V. Efremov, K. Goeke, S. Menzel, A. Metz, and P. Schweitzer, Phys. Rev. D **73**, 014021 (2006).
- [26] M. Anselmino *et al.*, *Transversity 2005* (World Scientific, Singapore, 2006). [arXiv:0511017 [hep-ph]].
- [27] M. Anselmino, M. Boglione, U. D'Alesio, A. Kotzinian, F. Murgia, and A. Prokudin, Phys. Rev. D **71**, 074006 (2005); D **72**, 094007 (2005); D **72**, 099903(E) (2005); M. Anselmino, M. Boglione, U. D'Alesio, A. Kotzinian, S. Melis, F. Murgia, A. Prokudin, and C. Turk, Eur. Phys. J. A **39**, 89 (2009); M. Anselmino, M. Boglione, and S. Melis, Phys. Rev. D **86**, 014028 (2012).
- [28] W. Vogelsang and F. Yuan, Phys. Rev. D **72**, 054028 (2005).
- [29] Z. Lu, B. Q. Ma, and I. Schmidt, Phys. Lett. B **639**, 494 (2006); Phys. Rev. D **75**, 094012 (2007).
- [30] A. Bacchetta, F. Conti, and M. Radici, Phys. Rev. D **78**, 074010 (2008); A. Bacchetta, M. Radici, F. Conti, and M. Guagnelli, Eur. Phys. J. A **45**, 373 (2010).
- [31] Z. B. Kang, J. W. Qiu, W. Vogelsang, and F. Yuan, Phys. Rev. D **83**, 094001 (2011).
- [32] D. S. Hwang, J. Korean Phys. Soc. **62**, 581 (2013).
- [33] S. J. Brodsky, D. S. Hwang, Y. V. Kovchegov, I. Schmidt, and M. D. Sievert, Phys. Rev. D **88**, 014032 (2013).
- [34] M. G. Echevarria, A. Idilbi, Z. B. Kang, and I. Vitev, Phys. Rev. D **89**, 074013 (2014).
- [35] A. Martin, F. Bradamante, and V. Barone, Phys. Rev. D **95**, 094024 (2017).
- [36] T. Maji, D. Chakrabarti, and A. Mukherjee, Phys. Rev. D **97**, 014016 (2018).
- [37] M. Bury, A. Prokudin, and A. Vladimirov, Phys. Rev. Lett. **126**, 112002 (2021); JHEP **05**, 151 (2021).
- [38] X. Ji, Y. Liu, A. Schäfer, and F. Yuan, Phys. Rev. D **103**, 074005 (2021).
- [39] S. J. Brodsky and G. R. Farrar, Phys. Rev. Lett. **31**, 1153 (1973); V. A. Matveev, R. M. Muradyan, and A. N. Tavkhelidze, Lett. Nuovo Cimento Soc. Ital. Fis. **5**, 907 (1972).
- [40] S. J. Brodsky and S. D. Drell, Phys. Rev. D **22**, 2236 (1980).
- [41] S. J. Brodsky, D. S. Hwang, B. Q. Ma, and I. Schmidt, Nucl. Phys. B **593**, 311 (2001).
- [42] M. Glück, E. Reya, and A. Vogt, Eur. Phys. J. C **5**, 461 (1998).
- [43] M. Glück, E. Reya, M. Stratmann, and W. Vogelsang, Phys. Rev. D **63**, 094005 (2001).